ELSEVIER

Polymer 41 (2000) 4119–4125

polymer

Study of crystallization kinetics by temperature-modulated DSC☆

W. Chen[a,b], I.-K. Moon[a,b], B. Wunderlich[a,b,*]

[a]*Department of Chemistry, University of Tennessee, Knoxville, TN 37996-1600, USA*
[b]*Analytical and Chemical Sciences Division, Oak Ridge National Laboratory, Oak Ridge, TN 37831-6197, USA*

Received 13 May 1999; received in revised form 20 August 1999; accepted 24 August 1999

Abstract

A method of temperature-modulated differential scanning calorimetry (TMDSC), proposed by Toda et al., is used to study the crystallization kinetics of a polyester-imid, namely poly(4,4′-phthaloimidobenzoyldodecamethyleneoxycarbonyl). The polymer shows one irreversible melting/crystallization transition and one smaller, partially reversible transition. The experimental results prove that with this method one can obtain an important parameter that characterizes polymer crystallization via the temperature-dependence of the crystal-growth rate. The TMDSC data consist of the total heat flow, the magnitude of the apparent heat capacity, and the change of the phase lag of the heat flow in the transition region. No specific assumptions are made about the crystallization kinetics.

Keywords: Polymer crystallization; Reversible phase transition; Irreversible phase transition

1. Introduction

The recently developed temperature-modulated differential scanning calorimetry (TMDSC) has made a substantial impact on measuring various thermal responses and the understanding of their underlying kinetics and thermodynamics [1]. It is an important merit of the TMDSC method to allow a simultaneous measurement and subsequent deconvolution of the reversing and nonreversing thermal effects. For example, one can measure such nonreversing effects as the enthalpy relaxation during the glass transition, heats of chemical reaction, and heats of fusion and separate them quantitatively from the reversing heat capacity. The reversible thermodynamic heat capacity provides always the baseline for the quantitative evaluation of these nonreversing effects. Many applications have been established by linking the observed TMDSC signal to the kinetics of glass transition [2,3], melting [4–6], and the crystallization of polymers [7–10]. In this paper, as a part of our continuous effort in understanding the first-order transition by using TMDSC [1], a study of the crystallization kinetics of a polyester-imid has been carried out and will be reported.

2. Description of data treatment

The TMDSC method is well documented in Refs. [11–15]. Briefly, to the average sample temperature $\langle T_s \rangle$ an oscillation of $A_{T_s} \sin(\omega t + \varepsilon)$ is added, so that at steady state the sample temperature is given by:

$$T_s - T_0 = \langle q \rangle t - \frac{\langle q \rangle C_s}{K} + A_{T_s} \sin(\omega t + \varepsilon). \quad (1)$$

The average marked by $\langle\ \rangle$ is always taken over one modulation cycle, so that the modulation effect becomes zero. In Eq. (1) T_0 is the temperature at time $t = 0$; $\langle q \rangle$ the underlying, constant scanning rate; C_s, the heat capacity of the sample calorimeter (sample + pan); K, the Newton's law constant; A_{T_s}, the amplitude of temperature modulation; ω, the modulation frequency in rad s^{-1} ($=2\pi/p$ where p is the length of the modulation period in s); and ε, the phase lag relative to a reference oscillation. A similar expression can be written for the reference calorimeter with temperature T_r, heat capacity C_r, and phase lag ϕ. The differential heat flow $\dot{Q} = dQ/dt$ is then proportional to $\Delta T = T_r - T_s$ with a phase lag of δ, and can be derived from the general

☆ The manuscript has been authored by a contractor of the US Government under the contract No. DE-AC05-96OR22464. Accordingly, the US Government retains a non-exclusive, royalty-free license to publish, or reproduce the published form of this contribution, or allow others to do so, for US Government purposes.

* Corresponding author. Address: Department of Chemistry, University of Tennessee, Knoxville, TN 37996-1600, USA. Tel.: +1-423-974-0652; fax: +1-423-974-3419/54.

E-mail address: athas@utk.edu (B. Wunderlich).

0032-3861/00/$ - see front matter
PII: S0032-3861(99)00621-7

DSC equation [14,15]:

$$T_r - T_s = \frac{(C_s - C_r)}{K}\frac{dT_s}{dt} - \frac{C_r}{K}\frac{d(T_r - T_s)}{dt}. \quad (2)$$

For the solution of Eq. (2) the oscillating part of T_s and ΔT can be represented by the complex expressions:[1]

$$T_s^* A_{T_s} e^{i(\omega t+\varepsilon)}, \quad (3)$$

$$\Delta T^* = A_\Delta e^{i(\omega t+\delta)}. \quad (4)$$

The solution of Eq. (2) on insertion of Eqs. (3) and (4) leads to the two basic TMDSC equations for the reversing part of the experiment [14,15]:

$$\cos(\varepsilon - \delta) = \frac{KA_\Delta}{A_{T_s}\omega(C_s - C_r)}, \quad (5)$$

$$|(C_s - C_r)| = \frac{A_\Delta}{A_{T_s}}\sqrt{\left(\frac{K}{\omega}\right)^2 + C_r^2} \quad (6)$$

where A_Δ is the amplitude of the temperature difference ΔT in response to the modulation of the sample temperature, T_s. The reversing heat capacity measured in this fashion represents the thermodynamic heat capacity as long as the sample response is fast relative to the frequency of modulation, ω. If the sample response is slow, as is possible during transitions, an additional phase lag α may arise:

$$\alpha = (\varepsilon - \delta) - (\varepsilon_o - \delta_o) \quad (7)$$

where ε_o and δ_o are extrapolated from outside of the transition region to the temperature of interest. The measured heat capacity, in turn, becomes an apparent heat capacity, describable also as a complex quantity. In the transition region, the heat flow to and from the sample can be represented by the sum of the contribution from heat capacity (mc_p) and from the exo- or endothermic heat flow of transformation, $F(t, T_s)$:

$$\frac{dQ}{dt} \equiv \dot{Q} = -mc_p\frac{dT_s}{dt} + F(t, T_s). \quad (8)$$

Since the rate of transformation is a function of supercooling or superheating, the heat flow can be expanded about the sample temperature for the case of sufficiently small modulation [7,11–13,16]:

$$F(t, T_s) \equiv -\frac{d(\Delta H)}{dt} = \langle F\rangle(t, \langle T_s\rangle) + F'_T A_{T_s} e^{i(\omega t+\varepsilon)} + \cdots \quad (9)$$

where $\langle F\rangle(t, < T_s\rangle)$ is the heat flow at time t, averaged over one modulation period, which represents the heat of transformation due to the underlying linear temperature change, and $F' = \partial F/\partial T$ represents the temperature coefficient of the heat flow. Since the second term in the expansion describes the modulation components of the heat flow *and* the contribution from the heat capacity, the oscillating term in Eq. (8) is [7]:

$$A_{\dot{Q}} e^{i(\omega t+\delta)} = -mc_p\frac{d}{dt}A_{T_s} e^{i(\omega t+\varepsilon)} + F'_T A_{T_s} e^{i(\omega t+\varepsilon)} \quad (10)$$

where $A_{\dot{Q}} e^{i(\omega t+\delta)}$ represents the amplitude of the modulated terms of the heat flow. By rearranging the relationship, one obtains the expression of the amplitude of the apparent heat capacity in the transformation region, A_{C_p} [7]:

$$A_{C_p} e^{-i\alpha} \equiv A_{C_p}\cos\alpha - iA_{C_p}\sin\alpha = mc_p + \frac{i}{\omega}F'_T. \quad (11)$$

Eq. (11) is the basic equation for data treatment for any thermal transformations investigated by the TMDSC technique.

3. Model for polymer crystallization

Polymer crystallization is a process of nucleation and growth. The development of crystallinity with time can be described by specific models that take into account the morphology of the crystals, such as the Avrami equation [17]. These models become, however, rather complicated and need detailed information about nucleation and crystal morphology. Instead, Toda et al. proposed a simple rate of transformation R, that is directly proportional to the crystal growth rate G, multiplied with the total area of the growth surface, S_{total}, which should hold at any instant [7], i.e.:

$$R = GS_{total}. \quad (12)$$

Setting the enthalpy change per unit volume equal to Δh, the heat flow of the transition can be represented by:

$$F = \Delta hR = \Delta hGS_{total}. \quad (13)$$

Normally, polymer crystallization requires a high degree of supercooling (ca. 10 K). Therefore, for small temperature modulations (ca. 0.2 K), the response of the transformation is only a periodic change in the crystal growth rate $G(T_s)$. The total area of the growth faces, S_{total}, on the other hand, does not change significantly during the chosen small modulation amplitudes. As a result, one can write for the temperature dependence of the latent heat flow:

$$F'_T \equiv \frac{\partial F}{\partial T} - \Delta hS_{total}\frac{dG(T_s)}{dT}. \quad (14)$$

Combing Eqs. (13) and (14) and substituting F'_T from Eq. (11) then results in:

$$\frac{d\ln G(T_s)}{dT} = \frac{F'_T}{F} = -\frac{\omega A_{C_p}\sin\alpha}{F}. \quad (15)$$

The temperature dependence of the crystal growth rate can be determined, thus, from Eq. (15). It should be noticed, that the unit of $d\ln G/dT$ as expressed in Eq. (15) is K^{-1}. In this work, the temperature dependence of the crystal growth rate of a polyester-imid was investigated using this approach.

[1] Note that the phase lags ε and δ are different by $\pi/2$ in opposite directions relative to the derivations in Ref. [14] to agree with that used by Toda et al.

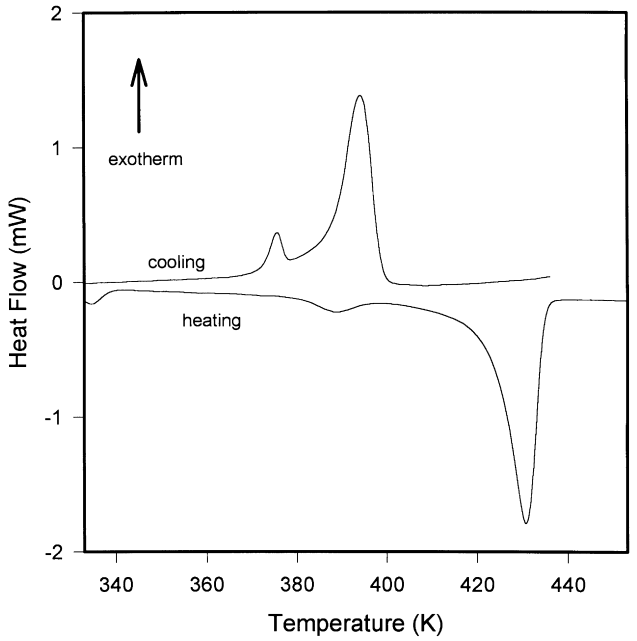

Fig. 1. Conventional DSC traces of PEIM-12 with scanning rates of ± 10 K min^{-1}. A 35 K supercooling is observed in the crystallization.

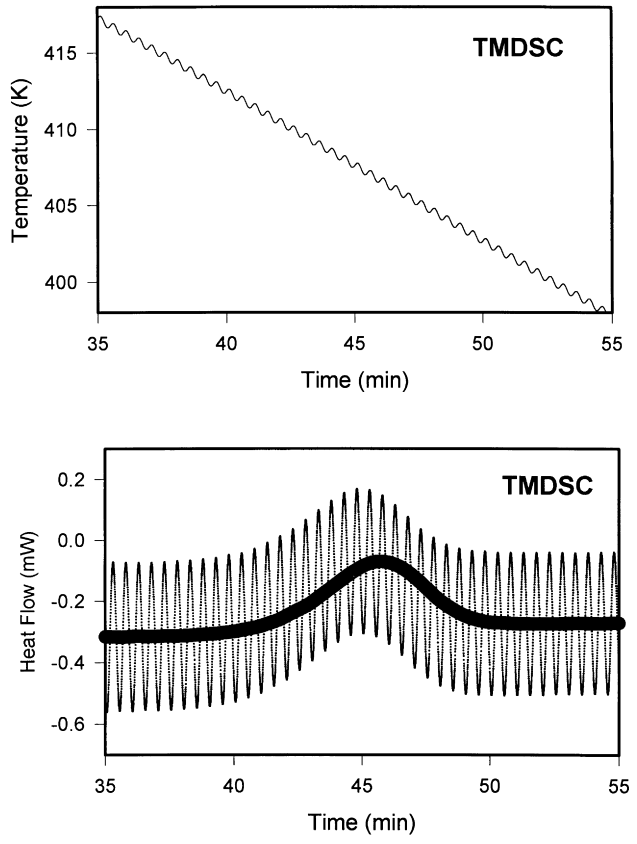

Fig. 2. Raw data of TMDSC for PEIM-12 crystallization measured with a 2.0 K min^{-1} underlying linear cooling, a ± 0.1 K modulation amplitude and 30 s period. The thick line represents the total heat flow, obtained by performing a sliding average of the modulated heat flow over each modulation period. The smaller, low-temperature transition is not included in this figure.

4. Experimental

In the present work, the Thermal Analyst 2910 MDSC™ system with a liquid-nitrogen cooling accessory from TA Instruments Inc. was used. Dry nitrogen gas with a flow rate of 20 ml min^{-1} was purged through the DSC cell. The temperature of the TMDSC equipment was initially calibrated in the standard DSC mode at 10 K min^{-1} by using the onsets of the transition peaks for cyclohexane (186.09 and 297.7 K), octane (216.15 K), water (273.15 K), and indium (429.75 K). The heat flow was calibrated with the heat of fusion of indium (28.45 J g^{-1}).

The TMDSC experiments were performed with underlying scanning rates $\langle q \rangle = 2.0$ K min^{-1} and a temperature-modulation amplitude $A_{T_s} = 0.1$ K. Modulation periods $p = 30$, 60, 90 s were chosen in the corresponding experiments. All the TMDSC data were averaged over three measurements in each experimental condition to ensure the data quality.

The polymer under investigation is poly(4,4′-phthaloimidobenzoyldodecamethyleneoxycarbonyl) (PEIM-12):

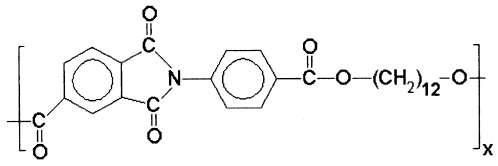

The sample was synthesized as described in Refs. [18,19] and had an inherent viscosity of 0.91 dl g^{-1} (measured in CH_2Cl_2/TFA of 4:1 volume ratio at 293 K). The samples were analyzed as received. The detailed investigation of PEIM-12 by solid state NMR, Wide-angle X-ray, as well as standard DSC proved that below the isotropization temperature, PEIM-12 crystallizes into a semicrystalline condis crystal (conformationally disordered crystal) and its "smectic-like" layer structure is due to nanophase separation of the polar mesogenic groups and the nonpolar methylene groups [20]. The sample was pressed into thin films (ca. 0.015 mm in thickness) for optimum thermal conduction with the sample pan. The sample weight was 3.00 mg.

5. Results

Fig. 1 shows the conventional DSC traces of PEIM-12 taken with 10 K min^{-1} linear heating/cooling rates. On heating, there are two first-order endothermal transitions. An initial disordering occurs at $T_d \approx 390$ K and the ultimate isotropization occurs at $T_i = 431.2$ K, respectively (peak temperatures). On cooling, two endothermic transitions were observed at $T_{c1} = 396.5$ K and $T_{c2} = 373.4$ K. These data agree with our previous heat capacity and heat of transition studies on the same PEIM-12 sample [20]. Fig. 1 indicates that there is a strong supercooling on crystallization of PEIM-12 (ca. 35 K) for both transitions, although the

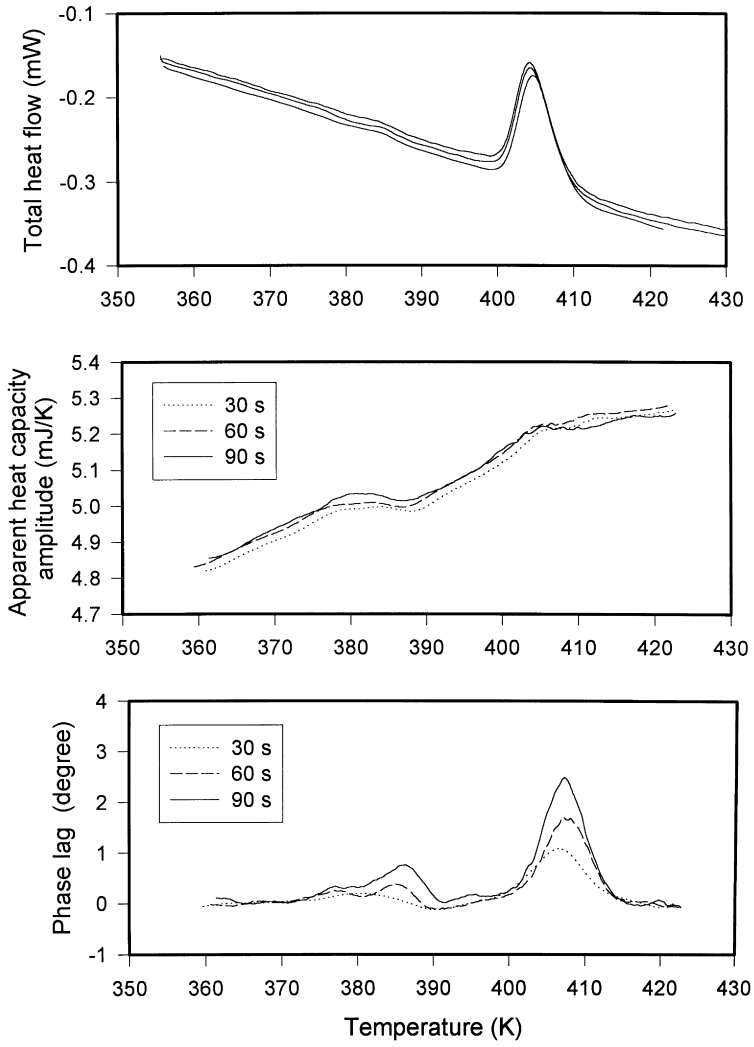

Fig. 3. Results of TMDSC on PEIM-12 crystallization with three different modulation frequencies. The top graph shows the total heat flow. The middle plots indicate the apparent heat capacity amplitude, A_{C_p}, calculated with Eq. (6). The bottom plots depict the phase lag α in the transition regions as calculated with Eq. (7).

low-temperature ordering overlaps in its final part with the beginning of disordering at about 370 K.

Fig. 2 represents the raw data of the PEIM-12 crystallization, measured by TMDSC with a 2.0 K min^{-1} underlying linear cooling and a $\pm$0.1 K temperature modulation with a 30 s modulation period. The upper plot is the sample-temperature profile, T_s, during the measurement. The lower plot is the instantaneous, modulated heat-flow corresponding to the temperature change shown in the upper plot. The thick line in the lower plot is the total heat flow obtained by forming the sliding average of the modulated heat flow over $\pm 1/2p$. The total heat flow measured in TMDSC is largely equivalent to that of the conventional DSC measurement [11–15]. Converting the time scale in Fig. 2 into $\langle T_s \rangle$ one finds that the crystallization begins at about 410 K in the TMDSC measurement. The supercooling is reduced to 20 K because of the lower cooling rate compared to the DSC data shown in Fig. 1. The second, smaller exothermic transition shown in Fig. 1 is not included in the temperature range of Fig. 2.

Fig. 3 depicts the TMDSC measurements of PEIM-12 on cooling with three different modulation frequencies ($p = 30$, 60, and 90 s). The top plots are the total heat flow curves of the three measurements. Obviously, the total heat flows from the three measurements are identical. Shown in Fig. 3 is a small vertical shift of the DSC traces due to a baseline drift. Such observations prove that the sample keeps practically the same thermal history in measurements with different modulation periods. The middle plots in Fig. 3 are the apparent heat capacity amplitudes A_{C_p} calculated from the total and reversible heat flows of Fig. 2, using Eq. (6). The reversing heat-flow was taken, as is usual, as the first harmonic of the Fourier series that describes the raw data of Fig. 2 [11–15]. The A_{C_p} shows little change for the different modulation frequencies, but indicates different responses as a function of temperature for

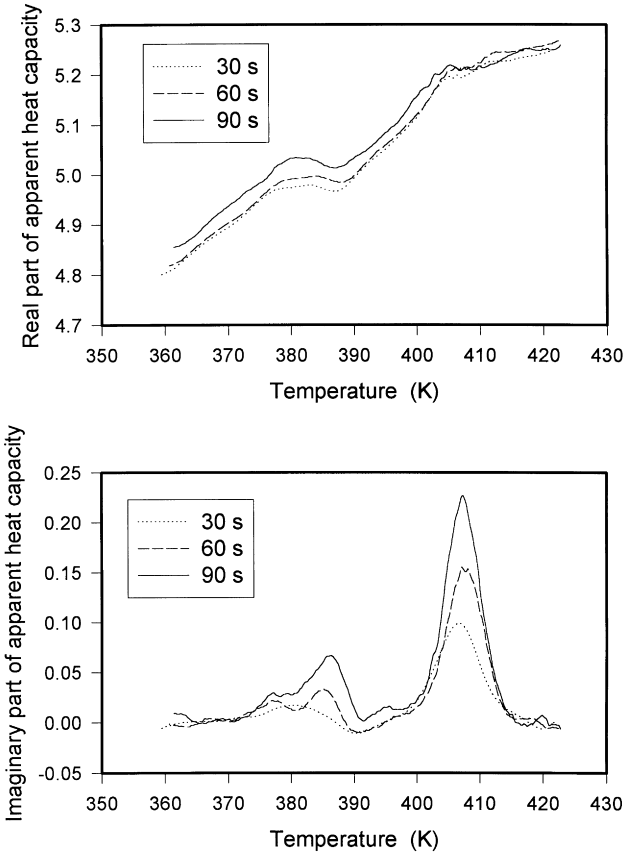

Fig. 4. The real and imaginary parts of the complex apparent heat capacity calculated using Eq. (11). The real part of the apparent heat capacity in the upper plot shows no frequency dependence.

the two ordering transitions. The bottom plots in Fig. 3 depict the changes in phase lag α in the transition region, calculated using Eq. (7). The phase lag ($\varepsilon - \delta$) was determined from the raw data of modulated sample temperature and heat flow [7,14]. The phase lag in the transition regions shows a strong frequency dependence in both transitions.

Using the amplitudes of the apparent heat capacity, A_{C_p}, and the phase lag, α, from Fig. 3, one can calculate the real and imaginary parts of the complex, apparent heat capacity, represented by Eq. (11). Fig. 4 illustrates that the so calculated real parts of the apparent heat capacities show little or no frequency dependence (upper plots), while the calculated imaginary parts (lower plots) show a strong frequency dependence in the transition regions. The changes as a function of temperature are similar to the changes in the corresponding graphs in Fig. 3 of the apparent heat capacity amplitudes and phase lags.

6. Discussion

6.1. High-temperature crystallization peak

The supercooling of about 20 K observed during the TMDSC measurements (see Fig. 2) ensures that the small temperature modulation ($A_{T_s} = 0.1$ K) cannot induce any melting that corresponds to the high-temperature crystallization peak at T_{c1}. Therefore, the upper transition under investigation is expected to show only the crystallization process. The repeatable total heat-flow curves, shown in the top plots of Fig. 3, also confirm that the higher crystallization process is not affected by the change of modulation period. The amplitude of the reversing apparent heat capacity (the middle plots of Fig. 3) shows no frequency dependence. The same behavior was also observed in the major crystallization processes of polyethylene and poly(ethylene terephthalate) [7–10]. One can conclude that the amplitude of the apparent heat capacity, A_{C_p}, is insensitive to the modulation frequency during the crystallization processes. The phase lag α in the crystallization region, on the other hand, shows a strong frequency dependence (bottom plots in Fig. 3). Fig. 4 further illustrates the frequency dependence of the apparent heat capacity in plots of the real and imaginary parts of the apparent heat capacity as, calculated with Eq. (11). According to Eq. (11), the real part of the apparent heat capacity represents the true heat capacity of the studied sample if there is no melting occurring on the heating cycle. This real part of the heat capacity also should be independent of the modulation frequency since the heat capacity was proven to be able to response to temperature change much faster than the modulation frequency used in TMDSC [14,15].

There are, however, small glass-transition-like heat capacity decreases associated with the crystallization process between 415 and 405 K, indicating the change of the heat capacity from the value expected for the liquid to that for the semicrystalline solid. The imaginary part, represented by F'_T/ω of Eq. (11) shows, however, a strong frequency-dependence. This is also reasonable, because the F'_T represents the temperature coefficient of the total heat flow in the transformation region which carries the information about the time-dependent kinetics of the transformation [7].

Since the expected frequency dependence of the apparent heat capacity was confirmed by the data in Fig. 4, the temperature dependence of the crystal growth rate can be determined using Eq. (15). Fig. 5 illustrates the results of three different measurements carried out with different modulation frequency. The squares, circles and triangles represent the measurements with modulation periods of $p =$ 90, 60, and 30 s, respectively. The thin line in Fig. 5 denotes the total heat flow, plotted in arbitrary units to illustrate the temperature regions where the transitions occur. The second crystallization transition in the vicinity of 390 K is not visible in the total heat flow of Fig. 5 due to its small heat of transition (its position is marked by the arrow). In the first crystallization region between about 415 and 405 K, the $\mathrm{d}\ln G/\mathrm{d}T$ curve is almost horizontal, which agrees with the generally accepted linear growth rate model of polymer crystallization [17]. This plateau gradually decreases with temperature, indicating the typical temperature dependence

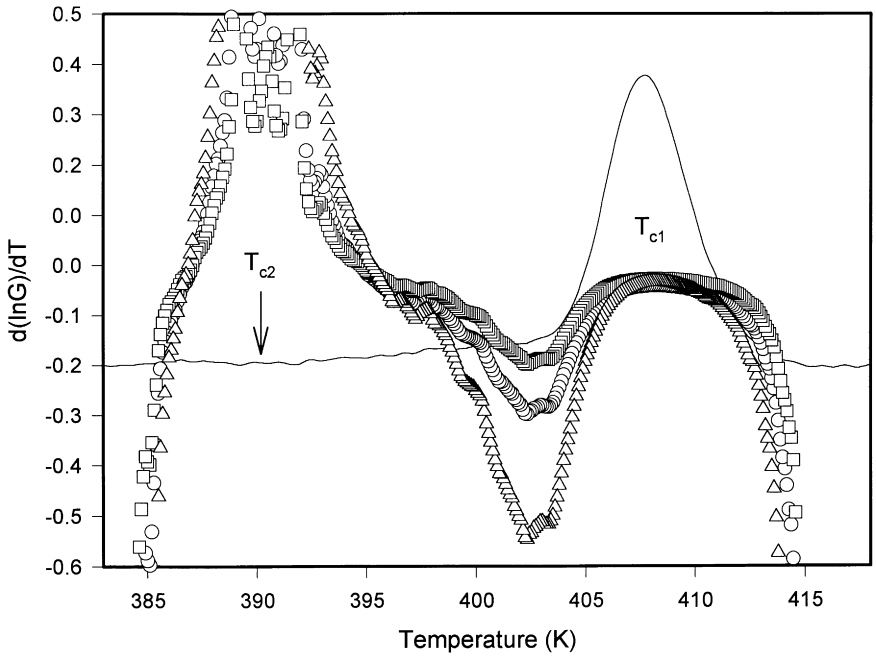

Fig. 5. Temperature dependence of the crystal growth rate determined using Eq. (15). The hollow squares, circles and triangles represent the measurements with modulation periods of 90, 60, and 30 s, respectively. The thin line curve is the total heat flow plotted in arbitrary units to show the temperature regions where the transitions occur.

of the crystal growth rate G. One expects a decrease in G as one decreases the supercooling and approaches the melting temperature at about 430 K [17]. All three measurements of different modulation frequencies superimpose within the transition, which agrees with the fact that d ln G/dT is determined by the crystallization kinetics of the sample and should be independent of the parameters of measurement. The sharp increase and decrease of d ln G/dT at the beginning and end of both transitions in Fig. 5 is caused by the vanishing signal outside of the transition region. The value of d ln G/dT is negative in the high-temperature crystallization region. It is well known that crystal growth rate of polymers has a bell-shape temperature dependence [17], i.e. d ln G/dT is negative when the polymers crystallize closer to the melting point and become positive when the polymer crystallizes closer to its glass transition. Finally, the data of PEIM-12 are of the same magnitude as the data reported by Toda et al. on polyethylene and poly(ethylene terephthalate), where the temperature dependence of the crystal-growth rate measured by TMDSC agrees with the data directly measured by optical microscopy [7–10]. Similarly, the values are in accord with a larger collection of linear crystal growth rates collected earlier [17].

6.2. Low-temperature crystallization peak

The temperature region of the low-temperature crystallization about T_{c2} shows a major difference relative to the high-temperature results. Although the total transition is small, it can be seen in Fig. 3 that there is an exotherm in both the total heat flow *and* the apparent heat capacity amplitude. Also, the exotherm in the apparent heat capacity amplitude (and the real part of the heat capacity of Fig. 4) may not be fully independent of the modulation amplitude. Despite these differences, during the second transition, Fig. 5 shows an elevated, horizontal region for d ln G/dT, even though the data scatter considerably due to the poor signal-to-noise ratio caused by the very small heats of transition. In connection with Fig. 1, which illustrates some overlap between the first disordering at T_d with the crystallization at T_{c2}, this low-temperature transition must be classified as partially reversible order/disorder transition, superimposed on the irreversible ordering as discussed in greater detail for linear-low-density polyethylenes [21]. In such cases, there is an additional contribution to the phase-lag baseline ($\varepsilon_o - \delta_o$) in the transition region from the thermally reversible mixed transition, which should be independent of the modulation frequency [6]. In order to obtain the correct d ln G/dT from Eq. (15), the phase lag α in Eq. (7) should be corrected for such additional contribution in the transition region using the approach proposed by Schick et al. [22,23]. In the present case the transition is not large enough to enable such separation.

Quite similarly small, reversible transitions were also discovered in other polymers and studied in our laboratory, such as poly(ethylene terephthalate) [24,25], poly(oxyethylene) [26,27], poly(trimethylene terephthalate) [28], poly(dioxanone) [29], and linear-low-density polyethylenes [21]. These polymers show much larger effects, particularly in low crystallinity and poorly crystallized samples. One can

thus identify such superposition of irreversible crystallization and some reversing ordering and disordering. The latter can further be separated into truly reversible transitions that give a constant contribution to the reversing heat capacity when extrapolated to infinite time at constant temperature over long times on quasi-isothermal analysis and slowly decreasing reversing contributions that indicate a crystal perfection on a slow time scale. Such observations are gained by long-times quasi-isothermal analysis, detailed in Ref. [21].

7. Conclusions

The temperature dependence of the crystal growth rate of a poly(4,4′-phthaloimidobenzoyl-dodecamethyleneoxycarbonyl) (PEIM-12) was studied by temperature-modulated differential scanning calorimetry, using the model proposed by Toda et al. [7]. Our experiments prove that this method can obtain this important parameter of polymer crystallization from the TMDSC data on the total heat flow, the amplitude of the apparent heat capacity, and the change of phase lag in the transition region. No details on the crystallization kinetics needed to be known. The analysis could also prove that the high-temperature transition is fully irreversible, while the low-temperature transition has a small, reversible component, as frequently observed for polymers.

Acknowledgements

The authors are grateful to Prof. A. Toda of the Hiroshima University for many detailed discussions with regard to the crystallization model used in this work and Prof. H.R. Kricheldorf of the University of Hamburg who supplied the PEIM-12. The work was supported by the Division of Materials Research, National Science Foundation, Polymers Program, Grant # DMR-9703692 and the Division of Materials Sciences, Office of Basic Energy Sciences, US Department of Energy at Oak Ridge National Laboratory, managed by Lockheed Martin Energy Research Corp. for the US Department of Energy, under contract number DE-AC05-96OR22464.

References

[1] Wunderlich B, Boller A, Okazaki I, Ishikiriyama K, Chen W, Pyda M, Pak J, Moon I, Androsch R. Thermochim Acta 1999;330:21.
[2] Wunderlich B, Okazaki I. J Therm Anal 1997;49:57.
[3] Hatta I. Jpn J Appl Phys 1994;33:L686.
[4] Toda A, Tomita C, Hikosaka M, Saruyama Y. Polymer 1997;39:5093.
[5] Schawe JEK, Bergmann E. Thermochim Acta 1997;304:179.
[6] Chen W, Toda A, Moon I, Wunderlich B. J Polym Sci, Part B: Polym Phys 1999;37:1539.
[7] Toda A, Oda T, Hikosaka M, Saruyama Y. Thermochim Acta 1977;293:47.
[8] Toda A, Tomita C, Hikosaka M, Saruyama Y. Polymer 1997;38:2849.
[9] Toda A, Tomita C, Hikosaka M, Saruyama Y. Polymer 1997;39:1439.
[10] Toda A, Tomita C, Hikosaka M, Saruyama Y. Polymer 1997;38:231.
[11] Reading M, Elliott D, Hill VL. J Therm Anal 1993;40:949.
[12] Gill PS, Sauerbrunn SR, Reading M. J Therm Anal 1993;40:931.
[13] Reading M, Luget A, Wilson R. Thermochim Acta 1994;238:295.
[14] Wunderlich B, Jin Y, Boller A. Thermochim Acta 1994;238:277.
[15] Boller A, Jin Y, Wunderlich B. J Therm Anal 1994;42:307.
[16] Schawe JEK. Thermochim Acta 1995;260:1.
[17] Wunderlich B. Crystal nucleation, growth, annealing, Macromolecular physics, 2. New York: Academic Press, 1976.
[18] de Abajo J, de la Campa J, Kricheldorf HR, Schwarz G. Makromol Chem 1991;191:537.
[19] Kricheldorf HR, Schwarz G, de Abajo J, de la Campa J. J Polym 1991;32:942.
[20] Chen W, Pyda M, Habenschuss A, London JD, Wunderlich B. Polym Adv Technol 1997;8:747.
[21] Androsch R, Wunderlich B. Macromolecules 1999; in press.
[22] Schick C. Private communication.
[23] Weyer S, Hensel A, Schick C. Thermochim Acta 1997;304/305:267.
[24] Okazaki I, Wunderlich B. Macromolecules 1997;30:1758.
[25] Okazaki I, Wunderlich B. Macromol Chem Phys, Rapid Commun 1997;18:313.
[26] Ishikiriyama K, Wunderlich B. Macromolecules 1997;30:4126.
[27] Ishikiriyama K, Wunderlich B. J Polym Sci, Part B: Polym Phys 1997;35:1877.
[28] Pyda M, Wunderlich B. J Polym Sci, Part B: Polym Phys. Submitted.
[29] Ishikiriyama K, Pyda M, Zhang G, Forschner T, Grebowicz J, Wunderlich B. J Macromol Sci—Phys B 1998;37:27.